Journal of Applied Mechanics and Technical Physics, Vol. 48, No. 1, pp. 27–33, 2007

STABILIZATION AND EVOLUTION OF PARAMETERS OF A SYMMETRIC LAMINAR FLOW IN A PLANE CHANNEL WITH SUDDEN EXPANSION

A. M. Lipanov and S. A. Karskanov

UDC 519.6

A problem is formulated for computing the fields of parameters of a stationary laminar symmetric flow. A two-dimensional flow in a channel with a sudden change in the cross-sectional area is computed. The evolution of a three-dimensional perturbation inserted into the channel at the initial stage of computations is analyzed. It is demonstrated that the parameters of a two-dimensional flow in the channel at a Reynolds number $\mathrm{Re} = 50$ *become stabilized at a dimensionless time* $t > 20$*, whereas the steady state is reached under the same conditions at* $t \approx 100$*. At a distance of approximately* $10h$ *(*h *is the channel width at the entrance), the flow becomes one-dimensional, but the streamwise component of the velocity vector remains a function of the streamwise coordinate owing to flow compressibility.*

Key words: *equations of hydromechanics, Reynolds number, Mach number, separation region.*

Stationary laminar internal gas flows can be divided into symmetric and asymmetric. A symmetric flow is formed if the Reynolds number Re is low. It was shown [1] that the flow is symmetric at $\mathrm{Re} = 50$ but becomes asymmetric already at $\mathrm{Re} = 150$, though it remains stationary. It seems of interest to analyze the process of stabilization of laminar flow parameters and their variation along the channel in the case of a symmetric flow in a plane channel with a sudden increase in the cross-sectional area at the left boundary (Fig. 1).

The following system of three-dimensional equations of hydromechanics for a compressible medium was solved:

$$\frac{\partial \rho}{\partial t} + \frac{\partial \rho U}{\partial x} + \frac{\partial \rho V}{\partial y} + \frac{\partial \rho W}{\partial z} = 0; \tag{1}$$

$$\frac{\partial \rho U}{\partial t} + \frac{\partial}{\partial x}\left(P + \rho U^2\right) + \frac{\partial}{\partial y}\left(\rho U V\right) + \frac{\partial}{\partial z}\left(\rho U W\right)$$

$$= \frac{\partial}{\partial x}\left\{\mu\Big[\frac{4}{3}\frac{\partial U}{\partial x} - \frac{2}{3}\Big(\frac{\partial V}{\partial y} + \frac{\partial W}{\partial z}\Big)\Big]\right\} + \frac{\partial}{\partial y}\left[\mu\Big(\frac{\partial U}{\partial y} + \frac{\partial V}{\partial x}\Big)\right] + \frac{\partial}{\partial z}\left[\mu\Big(\frac{\partial U}{\partial z} + \frac{\partial W}{\partial x}\Big)\right],$$

$$\frac{\partial \rho V}{\partial t} + \frac{\partial}{\partial x}\left(\rho V U\right) + \frac{\partial}{\partial y}\left(P + \rho V^2\right) + \frac{\partial}{\partial z}\left(\rho V W\right)$$

$$= \frac{\partial}{\partial x}\left[\mu\Big(\frac{\partial U}{\partial y} + \frac{\partial V}{\partial x}\Big)\right] + \frac{\partial}{\partial y}\left\{\mu\Big[\frac{4}{3}\frac{\partial V}{\partial y} - \frac{2}{3}\Big(\frac{\partial U}{\partial x} + \frac{\partial W}{\partial z}\Big)\Big]\right\} + \frac{\partial}{\partial z}\left[\mu\Big(\frac{\partial V}{\partial z} + \frac{\partial W}{\partial y}\Big)\right], \tag{2}$$

Institute of Applied Mechanics, Ural Division, Russian Academy of Sciences, Izhevsk 426067; elle@udman.ru.
Translated from Prikladnaya Mekhanika i Tekhnicheskaya Fizika, Vol. 48, No. 1, pp. 35–42, January–February, 2007. Original article submitted April 19, 2006; revision submitted July 18, 2006.

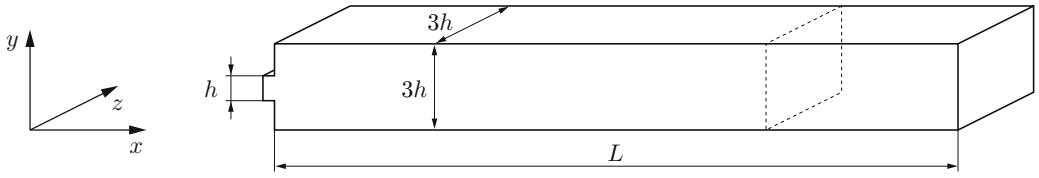

Fig. 1. Domain of integration.

$$\frac{\partial \rho W}{\partial t} + \frac{\partial}{\partial x}(\rho W U) + \frac{\partial}{\partial y}(\rho W V) + \frac{\partial}{\partial z}(P + \rho W^2)$$

$$= \frac{\partial}{\partial x}\Big[\mu\Big(\frac{\partial U}{\partial z} + \frac{\partial W}{\partial x}\Big)\Big] + \frac{\partial}{\partial y}\Big[\mu\Big(\frac{\partial V}{\partial z} + \frac{\partial W}{\partial y}\Big)\Big] + \frac{\partial}{\partial z}\Big\{\mu\Big[\frac{4}{3}\frac{\partial W}{\partial z} - \frac{2}{3}\Big(\frac{\partial U}{\partial x} + \frac{\partial V}{\partial y}\Big)\Big]\Big\};$$

$$\frac{\partial \rho E}{\partial t} + \frac{\partial}{\partial x}[(P + \rho E)U] + \frac{\partial}{\partial y}[(P + \rho E)V] + \frac{\partial}{\partial z}[(P + \rho E)W]$$

$$= -\frac{2}{3}\frac{\partial}{\partial x}\Big[\mu U\Big(\frac{\partial U}{\partial x} + \frac{\partial V}{\partial y} + \frac{\partial W}{\partial z}\Big)\Big] + 2\frac{\partial}{\partial x}\Big(\mu U\frac{\partial U}{\partial x}\Big) + \frac{\partial}{\partial x}\Big[\mu V\Big(\frac{\partial U}{\partial y} + \frac{\partial V}{\partial x}\Big)\Big]$$

$$+ \frac{\partial}{\partial x}\Big[\mu W\Big(\frac{\partial U}{\partial z} + \frac{\partial W}{\partial x}\Big)\Big] + \frac{\partial}{\partial y}\Big[\mu U\Big(\frac{\partial U}{\partial y} + \frac{\partial V}{\partial x}\Big)\Big] + \frac{\partial}{\partial y}\Big[\mu W\Big(\frac{\partial V}{\partial z} + \frac{\partial W}{\partial y}\Big)\Big]$$

$$- \frac{2}{3}\frac{\partial}{\partial y}\Big[\mu V\Big(\frac{\partial U}{\partial x} + \frac{\partial V}{\partial y} + \frac{\partial W}{\partial z}\Big)\Big] + 2\frac{\partial}{\partial y}\Big(\mu V\frac{\partial V}{\partial y}\Big) + \frac{\partial}{\partial z}\Big[\mu U\Big(\frac{\partial U}{\partial z} + \frac{\partial W}{\partial x}\Big)\Big]$$

$$+ \frac{\partial}{\partial z}\Big[\mu V\Big(\frac{\partial V}{\partial z} + \frac{\partial W}{\partial y}\Big)\Big] - \frac{2}{3}\frac{\partial}{\partial z}\Big[\mu W\Big(\frac{\partial U}{\partial x} + \frac{\partial V}{\partial y} + \frac{\partial W}{\partial z}\Big)\Big] + 2\frac{\partial}{\partial z}\Big(\mu W\frac{\partial W}{\partial z}\Big)$$

$$+ \frac{\partial}{\partial x}\Big(\lambda\frac{\partial T}{\partial x}\Big) + \frac{\partial}{\partial y}\Big(\lambda\frac{\partial T}{\partial y}\Big) + \frac{\partial}{\partial z}\Big(\lambda\frac{\partial T}{\partial z}\Big). \tag{3}$$

Here t is the time, x, y, and z are the Cartesian coordinates, U, V, and W are the velocity-vector components, T is the temperature, ρ is the density, P is the pressure, E is the total internal energy, μ is the viscosity, and λ is the thermal conductivity. The values of μ and λ were assumed to be constant.

Equations (1)–(3) were written in dimensionless form by using the following scales: the distance between the surfaces at the channel entrance h, the maximum value of the streamwise component of the velocity vector at the channel entrance $\hat{U}$, and the gas pressure and density at the channel entrance $\hat{P}$ and $\hat{\rho}$ corresponding to $\hat{U}$.

Equations (1)–(3) are written in divergent form; therefore, the variables in partial derivatives are omitted.

In Eq. (3), we have

$$E = \frac{U^2 + V^2 + W^2}{2} + c_V T \tag{4}$$

(c_V is the specific heat at constant volume).

Using the equation of state of an ideal gas $P = \rho RT$ and the relation $c_p = c_V + R$, we can write Eq. (4) as

$$E = \frac{U^2 + V^2 + W^2}{2} + \frac{1}{k-1}\frac{P}{\rho},$$

where $k = c_p/c_V$ (c_p is the specific heat at constant pressure) and R is the universal gas constant.

The following initial conditions are used in solving Eqs. (1)–(3):

$$U = V = W = 0, \qquad P = P_{\text{in}}, \qquad T = T_{\text{in}}.$$

The boundary conditions at the channel entrance are

$$P_0 = s_0\rho_0^k;$$

$$U_0 = \varphi(y, \delta_U) + C_1(P_0 - \langle P\rangle)\varphi(y, \delta_T), \tag{5}$$

where

$$\varphi(y,\delta_\xi)=\begin{cases}1-(1-y/\delta_\xi)^N, & 0\leqslant y\leqslant\delta_\xi,\\ 1, & \delta_\xi<y\leqslant h-\delta_\xi,\\ 1-((y-h+\delta_\xi)/\delta_\xi)^N, & h-\delta_\xi<y\leqslant h,\end{cases}$$

$\xi\to(U,T)$, δ_U and δ_T are the thicknesses of the dynamic and thermal boundary layers, respectively, s_0 is the specific entropy, $\langle P\rangle$ is the mean pressure P_0 at the channel entrance, $C_1=1/(k\mathrm{M}_0)$, $\mathrm{M}_0=U_0/C_0$ is the Mach number, $C_0=(kP_0/\rho_0)^{1/2}$ is the velocity of sound, and N is the order of approximation inside the domain of integration.

The two remaining velocity-vector components equal zero:

$$V_0=W_0=0. \tag{6}$$

The boundary conditions at the channel exit are

$$P_L=P_a+C_2\sigma(t), \tag{7}$$

where P_a is the dimensionless ambient pressure,

$$C_2=\frac{k\mathrm{M}}{2H+\mathrm{M}\langle m\rangle(t)},\qquad \sigma(t)=m(L,t)-\langle m\rangle(t),$$

$$\langle m\rangle(t)=\frac{1}{L}\int\limits_S m(x,t)\,dx,\qquad m(x,t)=\iint\limits_{S(x)}\rho U\,dy\,dz,\qquad m(L,t)=\iint\limits_{S(L)}\rho U\,dy\,dz,$$

and H is the half-height of the channel.

It should be noted that the differences $P_0-\langle P\rangle$ and $m(L,t)-\langle m\rangle(t)$, in accordance with [2], are used to "remove" perturbations reaching the left and right boundaries of the domain of integration, respectively. If these differences are used, conditions (5) and (7) are nonstationary.

The boundary conditions on the wetted surfaces are

$$U=V=W=\frac{\partial T}{\partial n}=0.$$

As the domain of integration considered is a gap between two wetted surfaces, which is unbounded in the z direction, one of the planes (x,y) was chosen to correspond to the coordinate $z=0$ to obtain a finite-size volume. With allowance for the results of [1, 3], we used the periodicity conditions at a distance $\pm H_z$ from this plane:

$$U_+=U_-,\qquad V_+=V_-,\qquad W_+=W_-,\qquad P_+=P_-,\qquad \rho_+=\rho_-.$$

The distance $\pm H_z$ was chosen by the trial method; in the examples considered, $H_z=1.5h$.

Equations (1)–(3) were integrated in time by the second-order Runge–Kutta method. In terms of spatial variables, the first- and second-order partial derivatives were computed with eighth-order accuracy by Zalesak's method [4] in accordance to [1]. Difference grids with integration steps constant in space in the x,y,z directions were used.

The method used was tested for stability and convergence at $\mathrm{Re}=10^4$. In accordance with the approach described in [1], the convergence of the approximate solution was 0.1%.

A three-dimensional perturbation was set at the channel entrance at the initial stage of computations (first 100 steps of integration in time):

$$V_0=W_0=0.1U_0; \tag{8}$$

after that, conditions (6) were used.

The evolution of the third component W of the velocity vector can be estimated by analyzing the data in Fig. 2, which shows the behavior of W as a function of x and y for $z=0$ at different times. In Fig. 2a, the variable W corresponds to the time when its value at the channel entrance equals zero not only at the boundary but also in the nearest internal point (the condition $\partial W/\partial x=0$ holds at $x=0$). This condition is satisfied after 1700 steps of integration with respect to the dimensionless time ($t=3.4$) and corresponds to the Reynolds number $\mathrm{Re}=50$. In all computations, the Mach number was $\hat{\mathrm{M}}=0.6$. By that time, the leading front of the perturbation propagates into the channel to a distance $x\approx 3h$.

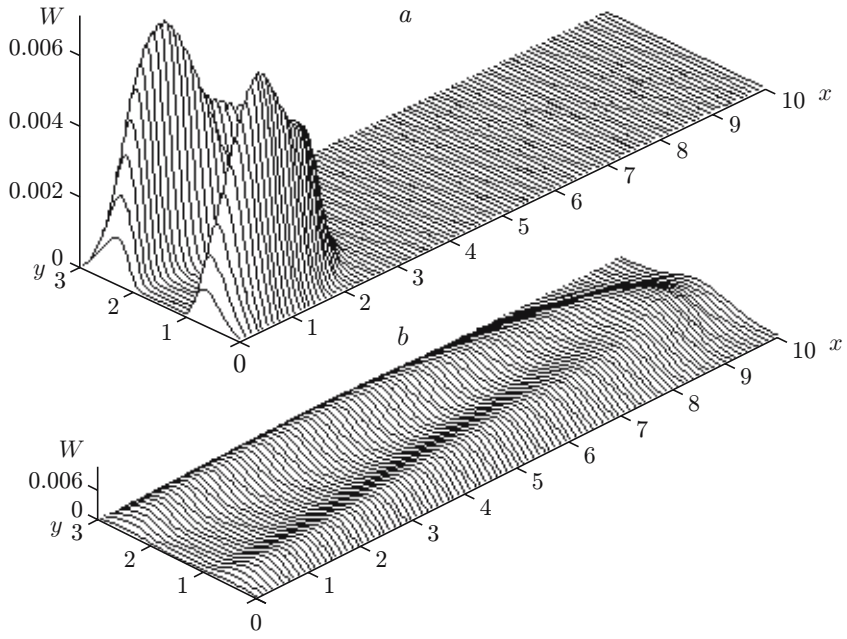

Fig. 2. Time evolution of the component W of the velocity vector at $\mathrm{Re} = 50$ and $t = 3.4$ (a) and 14.2 (b).

At a distance $y \approx 1.5h$, the leading front of the surface $W(x, y)$ drastically decreases with decreasing x. As $x \to 0$, the value of $W(x, y)$ remains close to zero. Surfaces beginning in separation regions are seen on the right and on the left of the front. Each of these surfaces has an extremum.

We can conclude that the perturbation is rather close to the channel entrance at the time corresponding to 100 steps of integration in time ($t = 0.2$).

The component W of the velocity vector evolves in time. Its spatial distribution, however, remains the same. The condition $\partial W/\partial x = 0$ holds at the channel entrance at $t > 3.4$, but the slope of the surface $W(x, y)$ and the maximum value of W become lower. The perturbation propagates downstream. At the time $t = 8$, the leading front of the perturbation is located at a distance $x \approx 55h$. The maximum value of W decreases by more than a factor of 3, as compared with its value at $t = 3.4$ (Fig. 2a). The maximum of the quantity W is located near the channel entrance. Later on, the surface $W(x, y)$ becomes less steep and has a maximum near its leading front (Fig. 2b), but the maximum value of W is smaller than that at $t = 3.4$ by an order of magnitude. Finally, the third component of the velocity vector vanishes at $t > 20$. At the right boundary of the domain of integration (Fig. 2b), the value of W does not exceed several digits in the fourth significant figure and can be neglected.

With increasing Re, the time needed for the velocity-vector component W to vanish increases. The function $W_{\max}(t, \mathrm{Re})$ can be approximated within 4% by the expression

$$W_{\max}(t, \mathrm{Re}) = f(t)[1 + \phi(\mathrm{Re})] + \varphi(\mathrm{Re}),$$

where $f(t) = a + b/t$, $a = -0.0093$, $b = 0.02265$,

$$\phi(\mathrm{Re}) = k\,\frac{\mathrm{Re} - \mathrm{Re}_0}{100}, \qquad \varphi(\mathrm{Re}) = c\left(\frac{\mathrm{Re} - \mathrm{Re}_0}{100}\right)^2 + d\,\frac{\mathrm{Re} - \mathrm{Re}_0}{100},$$

$k = 1.05$, $c = 0.01$, $d = 0.0035$, and $\mathrm{Re}_0 = 40$.

When a symmetric flow becomes two-dimensional (this occurs at the time $t \approx 20$ at $\mathrm{Re} = 50$), its parameters are still nonstationary. Figure 3 shows the time evolution of the streamwise component U of the velocity vector in a channel of length $L = 15h$ for $y = z = 0$ and $x = 12h$. It is seen that $U = 0.7$ at $t = 20$. With increasing t, the streamwise component U of the velocity vector first decreases and reaches a minimum ($U_{\min} = 0.456$) at $t = 38.34$. Then, the value of U increases again, reaches a maximum at $t = 56.2$, and acquires a constant level at $t \gtrsim 100$. The pressure behaves similarly.

Thus, we can conclude that the flow becomes stationary at $\mathrm{Re} = 50$ and $t > 100$.

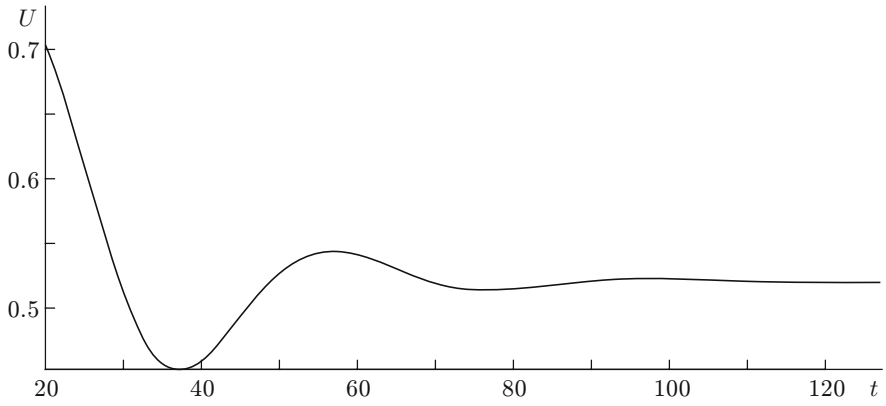

Fig. 3. Streamwise component of the velocity vector of the flow at the point $(12h, 0, 0)$ versus time.

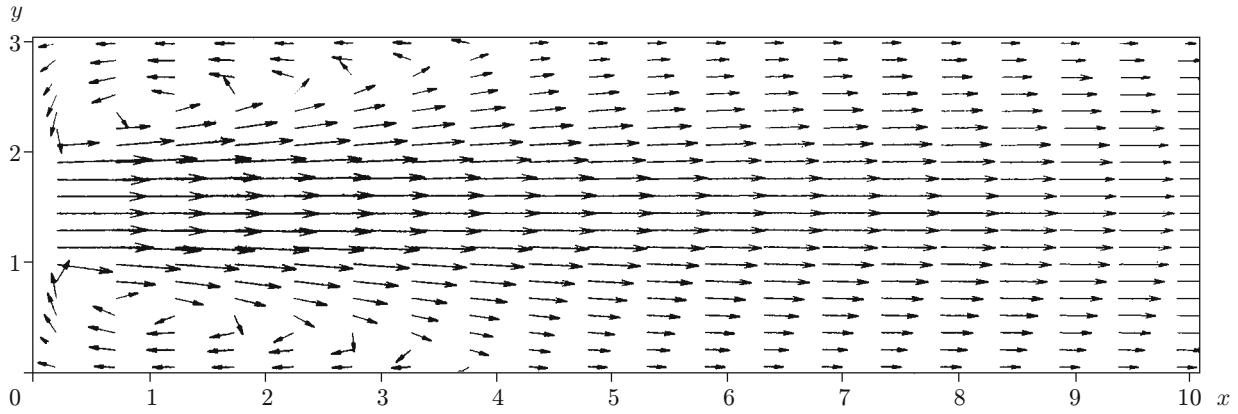

Fig. 4. Velocity vectors of the flow in the plane xy ($z = 0$) at $\mathrm{Re} = 60$.

Figure 4 shows the field of the velocity vectors of gas motion near the left boundary of the channel at $\mathrm{Re} = 60$. Separation zones are clearly visible. As Re increases, the separation regions become extended in the downstream direction. A two-dimensional gas flow is formed between the separation regions and the central part of the stream.

Near the left boundary of the channel, the vertical component of the velocity vector in the central part of the flow equals zero. Inside the separation regions, the value of this quantity is of the same order as the streamwise component. The length of the separation regions reaches $4h$. The velocity component V outside the separation regions rapidly decreases; it is smaller than 0.002 at a distance $x \approx 10h$ and tends to zero with increasing x.

Under the same conditions, the streamwise component of velocity also decreases with distance from the left boundary and reaches a minimum ($U_{\min} \approx 0.52$) at $x \approx 11.6h$ (Fig. 5).

The evolution of the profile $U(y)$ can be estimated on the basis of data plotted in Fig. 6: with increasing coordinate x, the change in the velocity U over the channel cross section is smaller. At $\mathrm{Re} = 40$, the profiles $U(y)$ for $x = 7h$ and $10h$ almost coincide. For $\mathrm{Re} = 50$ and 60, the difference in velocity profiles is more pronounced. The reason is that the streamwise coordinate U as a function of x varies over the entire channel length in a finite-length channel with the flow density and pressure varied in the streamwise direction (see Fig. 5).

For sufficiently long channels, the condition $\rho U = \mathrm{const}$ is valid for large values of x, but U is variable because ρ is variable. Therefore, the Poiseuille profile cannot be asymptotically obtained for a compressible medium. The difference is 2–3%.

The profile of the only (in a two-dimensional flow) component of the vorticity vector $\xi = \partial V/\partial x - \partial U/\partial y$ is symmetric, like the profiles of other flow parameters. The maximums of the component ξ correspond to the coordinates $y = h$ and $2h$ at $x = 0$. We have $\xi > 0$ at a distance $y = 2h$ and $\xi < 0$ at $y = h$. With increasing Re, the peaks of the vorticity vector ($x = 0$; $y = h$ and $2h$) become higher.

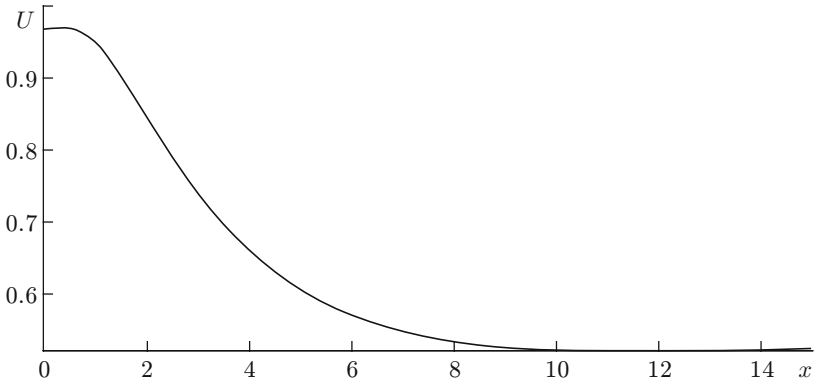

Fig. 5. Streamwise component of the velocity vector of the flow along the channel ($y = 0$, $z = 0$) at Re = 50 and M = 0.6.

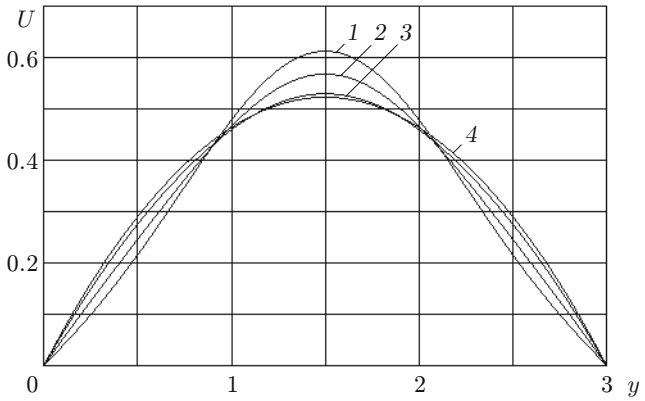

Fig. 6. Distribution of the streamwise component of the velocity vector over the channel height in different cross sections at Re = 40: $x = 4h$ (1), $5h$ (2), $7h$ (3), and $10h$ (4).

TABLE 1

Re	P_0	$P_{\max}$	x_*
40	0.945	1.025	4,57
50	0.929	1.013	5.58
60	0.920	1.008	6.50

TABLE 2

Re	T	
	$x = 0$	$x = L$
40	0.984	1.043
50	0.979	1.037
60	0.976	1.033

The vorticity vector decreases in the downstream direction and asymptotically tends to a limiting value corresponding to the greatest value of $\partial U/\partial y$.

Let us analyze the influence of temperature, pressure, and density. In a subsonic flow, these parameters vary insignificantly. The most significant change (up to 9.5%) is observed in pressure in the vicinity of the left boundary of the channel. The pressure first increases; after that, the pressure normalized to the ambient pressure passes through a maximum at a distance $x = x_*$ depending on Re and then it tends to unity on the right boundary of the channel. The values of pressure P_0 on the left boundary and $P_{\max}$ (at $x = x_*$), as well as the coordinates $x = x_*$, are listed in Table 1. With increasing Re, the values of P_0 and $P_{\max}$ decrease and the coordinate x_* is shifted inward the channel. The changes in pressure along the channel become less intense. Variations in density have the same character, but it changes to a smaller extent than pressure. At Re = 40, the density increases from $\rho = 0.96$ on the left boundary of the domain of integration to $\rho = 0.988$ at a point where $\rho = \rho_{\max}$. The change in density is approximately three times smaller than the change in pressure for the same value of Re. As Re increases,

the changes in density and pressure become more pronounced. At Re = 50, the density changes from 0.948 to 0.982, i.e., by 0.034, and the pressure changes by 0.084. At Re = 60, the density changes from 0.941 to 0.979, i.e., by 0.038, and the pressure increases by 0.088.

With increasing x, the temperature monotonically increases and asymptotically tends to the profile $T(y)$ corresponding to the stationary profile for the streamwise component of the velocity vector. The limits of variation of temperature of the subsonic core flow are greater than those for density but smaller than those for pressure (Table 2).

At Re = 40, the changes in pressure and density are 8.4 and 2.9%, respectively, whereas the temperature along the channel increases by 6%. At Re = 60, the corresponding values are 9.5, 4.0, and 5.8%.

REFERENCES

1. A. M. Lipanov, Yu. F. Kisarov, and I. G. Klyuchnikov, *Numerical Experiment in Classical Hydromechanics of Turbulent Flows* [in Russian], Izd. Ural. Otd. Ross. Akad. Nauk, Ekaterinburg (2001).
2. A. T. Fedorchenko, "Numerical study of subsonic flows of a viscous gas in a suddenly expanding channel," *Izv. Akad. Nauk SSSR, Mekh. Zhidk. Gaza*, No. 4, 32–41 (1988).
3. B. L. Rozhdestvenskii and I. N. Simakin, "Modeling of turbulent flows in a plane channel," *Zh. Vychisl. Mat. Mat. Fiz.*, **25**, No. 1, 96–121 (1985).
4. S. T. Zalesak, "A physical interpretation of the Richtmyer two-step Lax–Wendroff scheme, and its generalization to higher spatial order," in: *Advances in Computer Methods for Partial Differential Equations*, Proc. of the 5th IMACS Int. Symp. on Computer Methods for Partial Differential Equations (Bethlehem, June 19–21, 1984), Rutgers Univ. Press, New Brunswick (1984), pp. 491–496.